PROTEINS
STRUCTURE ■ FUNCTION ■ BIOINFORMATICS

The conformational plasticity of calmodulin upon calcium complexation gives a model of its interaction with the oedema factor of *Bacillus anthracis*

Elodie Laine,[1] Julliane D. Yoneda,[2] Arnaud Blondel,[1] and Thérèse E. Malliavin[1]*

[1] Unité de Bioinformatique Structurale, CNRS URA 2185 Institut Pasteur, 25–28, rue du Dr. Roux, Paris 75 724, France
[2] Programa de Posgraduaçao em Quimica Orgânica, Universidade Federal Fluminense, Outeiro de S. Joao Batista s/n, 24020150, Niteroi, RJ, Brazil

ABSTRACT

We analyzed the conformational plasticity of calmodulin (CaM) when it is bound to the oedema factor (EF) of Bacillus anthracis and its response to calcium complexation with molecular dynamics (MD) simulations. The EF-CaM complex was simulated during 15 ns for three different levels of calcium bound to CaM. They were respectively no calcium ion (EF–(Apo-CaM)), two calcium ions bound to the C-terminal domain of CaM (EF–(2Ca-CaM)), and four calcium ions bound to CaM (EF–(4Ca-CaM)). Calculations were performed using AMBER package. The analysis of the MD simulations illustrates how CaM forces EF in an open conformation to form the adenylyl cyclase enzymatic site, especially with the two calcium form of CaM, best suited to fit the open conformation of EF. By contrast, CaM encounters bending and unwinding of its flexible interlinker in EF–(Apo-CaM) and EF–(4Ca-CaM). Calcium binding to one domain of CaM affects the other one, showing a transmission of information along the protein structure. The analysis of the CaM domains conformation along the simulations brings an atomistic and dynamic explanation for the instability of these complexes. Indeed the EF-hand helices of the N-terminal domain tend to open upon calcium binding (EF–(4Ca-CaM)), although the domain is locked by EF. By contrast, the C-terminal domain is strongly locked in the open conformation by EF, and the removal of calcium induces a collapse of EF catalytic site (EF–(Apo-CaM)).

Proteins 2008; 71:1813–1829.

Key words: *calmodulin; Bacillus anthracis; oedema factor; molecular dynamics; calcium; solvent accessible surface; essential dynamics; NMR.*

INTRODUCTION

Structure flexibility plays a key role in target recognition for a large variety of proteins, in particular, for the ubiquitous protein calmodulin (CaM)[1] which participates in calcium signalling pathways that regulate many crucial biological functions. CaM actually played a historical role in the development of multidimensional NMR methods.[2–6] It is also a good model for understanding the implications of protein flexibility[7–10] and the thermodynamics of protein–protein interactions.[10–14]

CaM is composed of 148 residues and consists of two globular domains (lobes) connected by a flexible linker. Each domain can bind up to two calcium ions. The first crystallographic structures of mammalian CaM displayed a dumbbell-like shape for free CaM[15,16] and a compact conformation for CaM in complex with target peptides.[17] However, molecular dynamics (MD) simulations,[18–20] NMR experiments,[21,22] and a recent single-molecule study[23] revealed that free CaM is actually very flexible and there probably exist several conformational substrates in solution. Similarly, recent crystal structures[24,25] highlighted a variety of substates in the crystalline environment. The relationship between calcium ion complexation and biological activity was recently reviewed for the whole EF-hand protein family.[26,27]

Mostly, when CaM interacts with a target the lobes contact each other, forming a hydrophobic channel that engulfs the CaM-binding domain.[28–31] But the oedema factor (EF)-CaM complex,[32] which we discuss here, and other novel structures[33,34] have revealed an unexpected extended conformation of CaM.[35,36] EF is secreted by the Gram-positive spore-forming bacterium *Bacillus anthracis*, the etiological agent of anthrax. Activated as an adenylyl cyclase by CaM it produces cAMP from ATP in an uncontrolled fashion, and to this

Grant sponsors: French Ministry of Defence (DGA/MRIS), The National Scientific Research Centre (CNRS), The Pasteur Institute.
*Correspondence to: Thérèse E. Malliavin, Institut Pasteur, 25–28, rue du Dr. Roux, Paris 75 724, France. E-mail: terez@pasteur.fr
Received 13 June 2007; Revised 18 September 2007; Accepted 4 October 2007
Published online 3 January 2008 in Wiley InterScience (www.interscience.wiley.com).
DOI: 10.1002/prot.21862

Table I
Preparation Details of the MD Simulations

	EF–(Apo-CaM)	EF–(2Ca-CaM)	EF–(4Ca-CaM)	4Ca-CaM
Number of counterions	13	9	5	5
Water box dimensions		123.9 × 81.9 × 99.2 Å^3		57.5 × 64.0 × 76.1 Å^3
Number of water molecules	24,632	24,642	24,652	8,459
Total number of atoms	83,851	83,879	83,907	27,601

extent impairs the host immune defences.[37–40] Inhibiting the formation of the EF-CaM complex[41] is thus an important target to fight against anthrax toxicity.

The first X-ray structure of the EF-CaM complex displayed CaM in an extended conformation, loaded with two calcium ions and making extensive contacts with EF.[32] Since then Shen *et al.*[42] have solved several crystal structures of the complex, with different levels of calcium. These structures, together with a recent NMR study of free CaM and EF-bound CaM,[43] suggest that the level of calcium bound to CaM influences the stability and even the formation of the EF-CaM complex.

This work focuses mainly on CaM within the EF-CaM complex, as the internal motions of this protein deserve particular attention,[44] and the behavior of EF is presented in relation with CaM. The general purpose is to explore the mechanics of the EF-CaM interaction by perturbing the EF–(2Ca-CaM) complex, where the C-terminal lobe (sites 3 and 4) is loaded with two Ca^{2+}. Indeed it is experimentally deduced[43] that 2 Ca^{2+}-CaM has the highest affinity for EF, the complex with 4 Ca^{2+}-CaM being less stable and the complex with Apo-CaM not formed. CaM response to the perturbation of EF–(2Ca-CaM) is studied to relate this behavior to the knowledge on free CaM,[18–20,45] and a mechanical model of the EF-CaM interaction is proposed.

We report three 15-ns MD simulations of EF-CaM with different calcium complexations: EF–(Apo-CaM) with no calcium ion, EF–(2Ca-CaM) with two calcium ions bound to the C-terminal domain of CaM, and EF–(4Ca-CaM) with four calcium ions bound to CaM. It is worth mentioning that a previous MD study of the complex was performed by Zhao *et al.*[46] However the authors only considered the EF–(2Ca-CaM) complex, simulations were performed during a very short time period of 350 ps and a smooth cutoff was used for long-range interactions instead of the PME protocol.

The report is organized along two main axes. On the one hand, the trajectories are analyzed to validate them according to literature knowledge about the EF-CaM complex stability, CaM dynamics, and calcium affinity. On the other hand, the system perturbation induced by adding or removing a calcium ion is described and related to a model of the EF-CaM interaction.

MATERIALS AND METHODS

Preparation of initial coordinate files

Coordinates of the EF-CaM complex were obtained from the PDB entry 1K93.[32] Chains C (EF) and F (CaM) were selected, as they have the smallest number of missing residues. Residues 768 to 798, which comprised some disordered regions, were deleted. Coordinates of the released 4Ca-CaM were obtained from calmodulin X-ray structure in the EF–(4Ca-CaM) complex[42] (PDB id 1XFX: chain Q). Hydrogens were added using the LEaP module from AMBER 8.0[47] with the parm99 parameter set. Na^+ counterions were added to neutralize the system. The complex was then hydrated by a box of water molecules using a cutoff of 9 Å along the three axis, in order to discard any water molecule located further than 9 Å from any solute molecule. The TIP3P potential for water molecules[48] and periodic boundary conditions were used. Details are summed up in Table I.

Complexes with different levels of calcium were generated in the following way: the 1K93 structure produced the complexation with 2 Ca^{2+}, the EF–(Apo-CaM) complex was generated by removing the cations from 1K93, and the EF–(4Ca-CaM) complex was generated by adding 2 Ca^{2+} in the N-terminal calcium loops of CaM. The N-terminal domain of a recent free Ca^{2+}-loaded CaM structure[49] (PDB id: 1OOJ) was superimposed on the N-terminal domain of EF-bound CaM to position the calcium ions in the coordinating loops. Ions were Coulomb/Lennard-Jones parametrized (Van der Waals radius $R = 1.7131$ Å, well depth $\varepsilon = 0.459789$ kcal mol^{-1}).[50]

Molecular dynamics simulations

MD trajectories were calculated using AMBER 8.0[47] on an IBM cluster of Power 4 processors (IDRIS and CINES super computing centres). A cutoff of 9 Å was used for Lennard-Jones interactions, and long-range electrostatic interactions were calculated with the Particle Mesh Ewald (PME) protocol.[51] Temperature and pressure were regulated according to the Berendsen thermostat.[52]

Simulations were initiated by some rounds of semi-restrained and then unrestrained minimization of the entire system. Heating of the system was performed dur-

Table II
Comparison of Calcium Coordination Distances (Å) Calculated Between the N-Terminal Calcium Ions and the Corresponding Coordinating Atoms

	Free Ca^{2+}-CaM structure 100J[a]	EF–(4Ca-CaM) 1st equilibration[b]	EF–(4Ca-CaM) 2nd equilibration[c]
Site 1			
D20.Oδ1*	2.5	4.3	2.7
D20.Oδ2	4.2	2.6	2.6
D22.Oδ1	3.5	2.6	2.6
D22.Oδ2*	3.0	4.2	2.6
D24.Oδ1*	2.4	6.2	2.5
D24.Oδ2	4.2	7.9	4.4
T26.O*	2.6	2.8	2.6
E31.Oε1	2.7	6.6	8.5
E31.Oε2	2.5	5.3	7.3
Site 2			
D56.Oδ1*	2.7	2.6	2.7
D56.Oδ2	4.3	4.7	2.6
D58.Oδ1*	2.8	9.9	2.6
D58.Oδ2	3.9	9.0	4.1
N60.Oδ1*	2.6	8.7	3.1
T62.O*	2.6	9.9	2.8
E67.Oε1	2.7	11.3	5.2
E67.Oε2	2.9	10.8	4.8

During the second equilibration step, distance restraints were applied in each site between the flagged (*) atoms and the calcium position. Oε1 and Oε2 of E31, Oε1 and Oε2 of E67, which show larger distances than in free Ca^{2+}-CaM (pdb entry 1OOJ)[49] even after the second equilibration step, are also found far from the calcium ions in the crystallographic structure of EF–(4Ca-CaM) (pdb entry 1XFX),[42] at distances of 4.0 Å, 4.4 Å, 6.7 Å, and 4.6 Å.
[a]In the crystallographic structure of free Ca^{2+}-CaM (pdb entry 1OOJ).[49]
[b]In the EF–(4Ca-CaM) model, after the first equilibration step (without distance restraints).
[c]After the second equilibration step.

ing 10 ps up to 300 K at constant volume, while restraining the atoms of the complex (or calmodulin resp.) and the calcium positions with a force constant of 25 kcal mol^{-1} $Å^2$. The equilibration process was then performed in the following way: 1 MD round of 5 ps at constant volume and 4 MD rounds of 2.5 ps at constant pressure were run while reducing the position restraints from 25 kcal mol^{-1} $Å^2$ to 5 kcal mol^{-1} $Å^2$; eventually a last MD round of 10 ps was performed with a restraint of 2.5 kcal mol^{-1} $Å^2$.

For heating and equilibration of the EF–(4Ca-CaM) complex, no restraints were applied on the newly added calcium ions—neither on the CaM EF-hands coordination loops (residues 18–30 and 52–66), so that the system could better accommodate them. At the end of the equilibration process however, both N-terminal calcium ions were found far away from their initial positions (Table II). Hence a second equilibration was performed during 50 ps. Position restraints of 2.5 kcal mol^{-1} $Å^2$ were again applied on the whole system, except for calcium positions and the corresponding coordination loops. In addition, some specific distance restraints of 10 kcal mol^{-1} $Å^2$ were applied between the first Ca^{2+} and the oxygens Oδ1 of Asp 20, Oδ2 of Asp 22, Oδ1 of Asp 24, O of Thr 26 and between the second Ca^{2+} and the oxygens Oδ1 of Asp 56, Oδ1 of Asp 58, Oδ1 of Asn 60, O of Thr 62. As a result, most of the atoms in the coordination loops get as close from the calcium ions as in the X-ray structure 1OOJ[49] (Table II). However, atoms Oε1 and Oε2 of Glu 31, Oε1 and Oε2 of Glu 67 are found farther away from the calcium ions (4.8–8.5 Å), as it is also the case in the crystal structure 1XFX of EF–(4Ca-CaM).[42]

MD simulations were performed at temperature of 300 K and pressure of 1 atm during 15 ns. The SHAKE algorithm[53] was used to keep rigid all covalent bond involving hydrogens, enabling a time step of 2 fs. Atom coordinates were saved every ps (15,000 snapshots).

Analysis of the trajectories

To assess the convergence of the simulations we used the ensemble-based approach recently developed by Lyman and Zuckerman.[54] For each trajectory, it consists of generating a set of representative or "reference" structures and then clustering all the 15,000 conformations in corresponding "reference" groups.

An arbitrary cutoff r is first defined. A conformation is randomly picked up among the 15,000 conformations of the trajectory: this is the first "reference" structure. All conformations that show a RMSD from this "reference" structure smaller than r are removed from the trajectory. A second "reference" structure is picked up among the remaining conformations and again all conformations that show a RMSD smaller than r are removed. The operation is repeated until there is no remaining conformation. Finally, we obtain a set of "reference" structures that deviate from each other by at least r Å.

The trajectory is then split in two halves and conformations from each half are associated to their closest "reference" structure in terms of RMSD, constituting "reference" groups. If the simulation has converged, each "reference" structure must be represented by an equivalent number of conformations from both halves of the trajectory.

To compare this new method to a more traditional measurement, we computed the average time auto-correlation function on Cα atom positions:

$$C(t) = \frac{N!}{2!(N-2)!}\sum_{i=1}^{N-1}\sum_{j=i+1}^{N}\left\langle v_{ij}(t_0).v_{ij}(t_0+t)\right\rangle \quad (1)$$

where v_{ij} is the position vector between Cα atoms i and j and N is the number of Cα atoms. The obtained curve can be decomposed in exponential functions. For each simulation, $C(t)$ was fitted to an exponential model function $f(t) = c_1e^{-t/\tau_1} + c_2e^{-t/\tau_2} + c_3e^{-t/\tau_3}$[55] using XmGrace.[56]

A virtual dihedral angle (VDA), which describes the relative rotation of the lobes to each other, was calculated between the centres of mass of the four CaM EF-hands. Traditionally the VDA is taken as the pseudo-dihedral

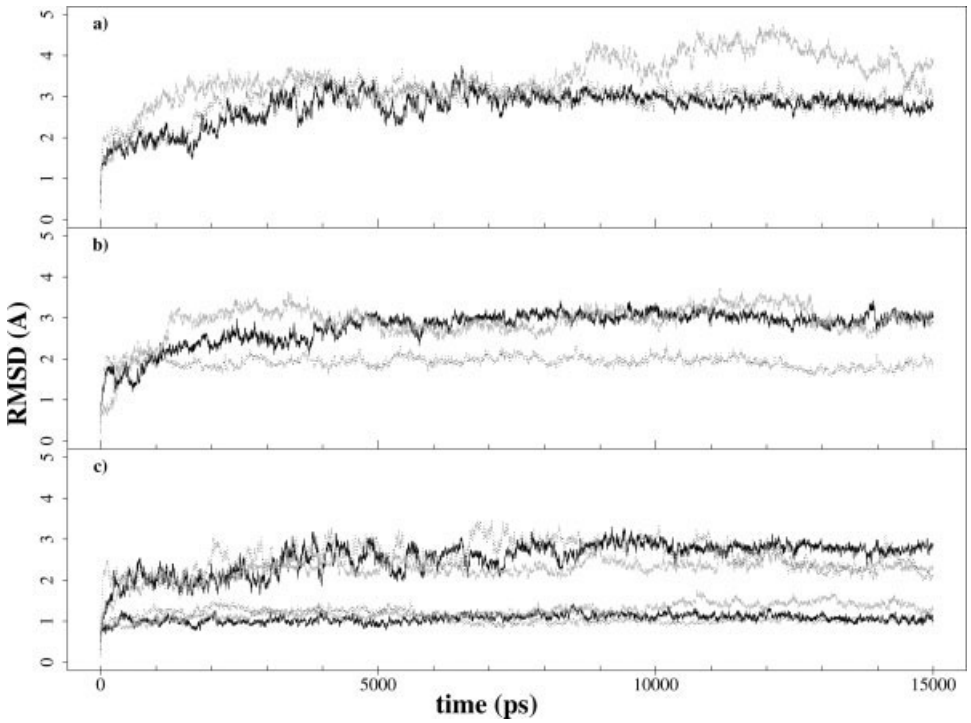

Figure 1

*Backbone RMSD of calmodulin with respect to the initial crystal structure (1K93)[32] (**a**) Total RMSD. (**b**) RMSD of the interlinker region using fit to residues 65–92. (**c**) RMSD of the N-terminal (up) and C-terminal domain (bottom) using independent fits to residues 5–64 and 92–147, respectively. In all plots, the EF–(Apo-CaM) trajectory is shown in grey (long dotted line), the EF–(2Ca-CaM) and EF–(4Ca-CaM) trajectories are shown in black (short dotted line and solid line, respectively).*

angle formed by the four calcium ions bound to CaM.[57] But, since this angle definition is relevant only for a straight central helix,[45] we used EF-hand centres of mass instead of calcium positions here.

The bending of the interlinker was evaluated by calculating the angle formed between the axes of α-helices IV (residues 64–72) and V (residues 86–94). Axes were defined with the successive middle points between atoms (i) N(i) and N(i+2), (ii) Cα(i), and Cα(i+2), (iii) C(i) and C(i+2), i being the residue index in the sequence. The EF-hand opening was evaluated in a similar way, from the angles between helices I (residues 8–19) and II (residues 31–37) in site 1, helices III (residues 46–53) and IV (residues 66–73) in site 2, helices V (residues 83–92) and VI (residues 103–110) in site 3, and helices VII (residues 119–127) and VIII (residues 139–145) in site 4.

Unless otherwise stated, trajectories were analyzed using the PTRAJ module of AMBER 8.0.[47] Determination of the secondary structure was performed by DSSP.[58] Electrostatic binding energies ΔE_{ele} of calcium ions were calculated with the MMPBSA module of AMBER 8.0.[47] SASA calculations were performed by MSMS[59] with a probe sphere radius of 1.5 Å. Interactions were identified with the HBPLUS 2.25 program[60] in the LIGPLOT 4.4.2 package.[61] VMD[62] was used for visualization and the analysis graphics were realised using the R package.[63]

RESULTS

To analyze CaM behavior in the EF-CaM complex, the following aspects were studied: (i) the relative stability of the different calcium levels; (ii) the influence of calcium level on calmodulin domain coupling and interaction with EF; (iii) the mechanics of the interaction between CaM and EF. In this work, we refer to the most recent MD simulations of free Apo-CaM[64] and Ca^{2+}-loaded CaM[19,20,65] in order to compare the conformational changes of EF-bound CaM to those of free CaM.

Relative stability of the EF-CaM complex for different levels of calcium

The relative stability of the different complexes was first investigated through an analysis of the convergence of the trajectories.

The conformational drift along the trajectories was evaluated by calculating the root mean square deviation (RMSD) of CaM coordinates from the initial coordinates (Fig. 1). Backbone RMS deviations stabilize at around

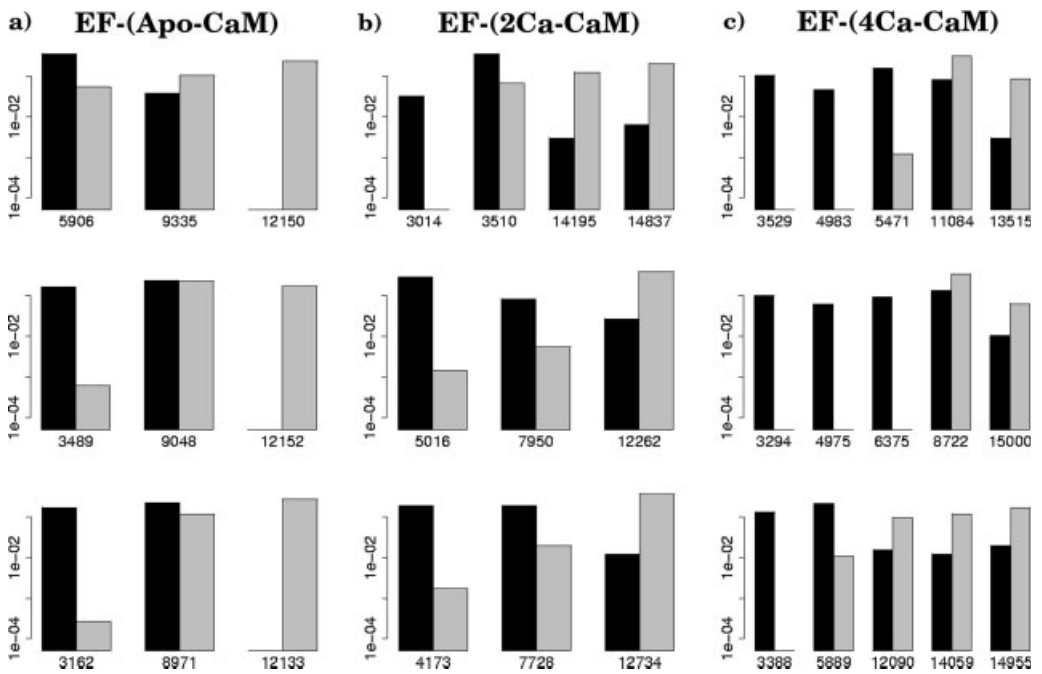

Figure 2

*Convergence analysis on the (**a**) EF–(Apo-CaM), (**b**) EF–(2Ca-CaM), and (**c**) EF–(4Ca-CaM) trajectories. Each line corresponds to an analysis for a given choice of the seed. The reference structures numbers are indicated in x-coordinates and correspond to their positions in ps along the trajectory. For each reference group are indicated the proportions of members in the first half (black bars) and in the second half (grey bars) of the trajectory.*

2.7 Å for EF–(2Ca-CaM) and EF–(4Ca-CaM) [Fig. 1(a)], whereas deviations for EF–(Apo-CaM) vary up to the end of the simulation in the 3.5–5 Å range. These values are small compared to RMSD values of free CaM, up to 15 Å,[19,20] because the amplitude of movement is reduced by EF. The RMS deviations calculated for EF (data not shown) are 3.7 Å (EF–(Apo-CaM)), 2.9 Å (EF–(2Ca-CaM)), and 4.1 Å (EF–(4Ca-CaM)): the smallest value is observed for the most experimentally stable complex.

Looking at Figure 1(c) we observe that the C-terminal domain (residues 93–147) is very stable with average RMSD between 1 and 1.5 Å whereas the RMSD is greater in the N-terminal domain (residues 5–64) up to 3 Å. Besides the RMSD of the whole protein and that of the domains are similar, indicating that, in complex with EF, global motions do not have the important contribution to the fluctuations that was found for free CaM.[19,20] We deduced from RMSD profiles [Fig. 1(a)] that 3 ns are necessary for the complex to relax from the initial crystallographic structure. These were thus removed for the convergence analysis and the latter study of CaM and EF.

To assess the convergence of the simulations in the last 12 ns we used the approach developed recently by Lyman and Zuckerman.[54] The robustness of the method was tested with different seeds for the conformation random picking up. In effect, results were similar for all seeds and we display here three analyses (Fig. 2).

Structural diversity proved to be limited in the trajectories as a cutoff of 3.5 Å was not sufficient to obtain more than one reference structure for EF–(2Ca-CaM) or EF–(Apo-CaM). Thus, a 2.5 Å cutoff was chosen, which enables to define three (or four) reference structures from EF–(Apo-CaM) [Fig. 2(a)] and EF–(2Ca-CaM) [Fig. 2(b)] and five reference structures from EF–(4Ca-CaM) [Fig. 2(c)].

EF–(2Ca-CaM) gives a good convergence criteria, since most of the reference structures are represented in both halves of the trajectory [Figs. 2(b) and 3(b)]. EF–(Apo-CaM) also, but to a lesser extent since the complex seems to explore an ensemble of new conformations near the end of the trajectory (12 ns) [Figs. 2(a) and 3(a)]. Concerning EF–(4Ca-CaM), conformations from the first half of the simulation are more represented than conformations from the second half [Figs. 2(c) and 3(c)].

The fitting of the average time auto-correlation functions onto exponential curves confirms that the EF–(4Ca-CaM) trajectory converges more slowly than the EF–(Apo-CaM) and EF–(2Ca-CaM) trajectories (Table III).

EF–(2Ca-CaM) is the only trajectory displaying at the same time one of the smallest drifts and a good convergence: this is in agreement with the stability experimen-

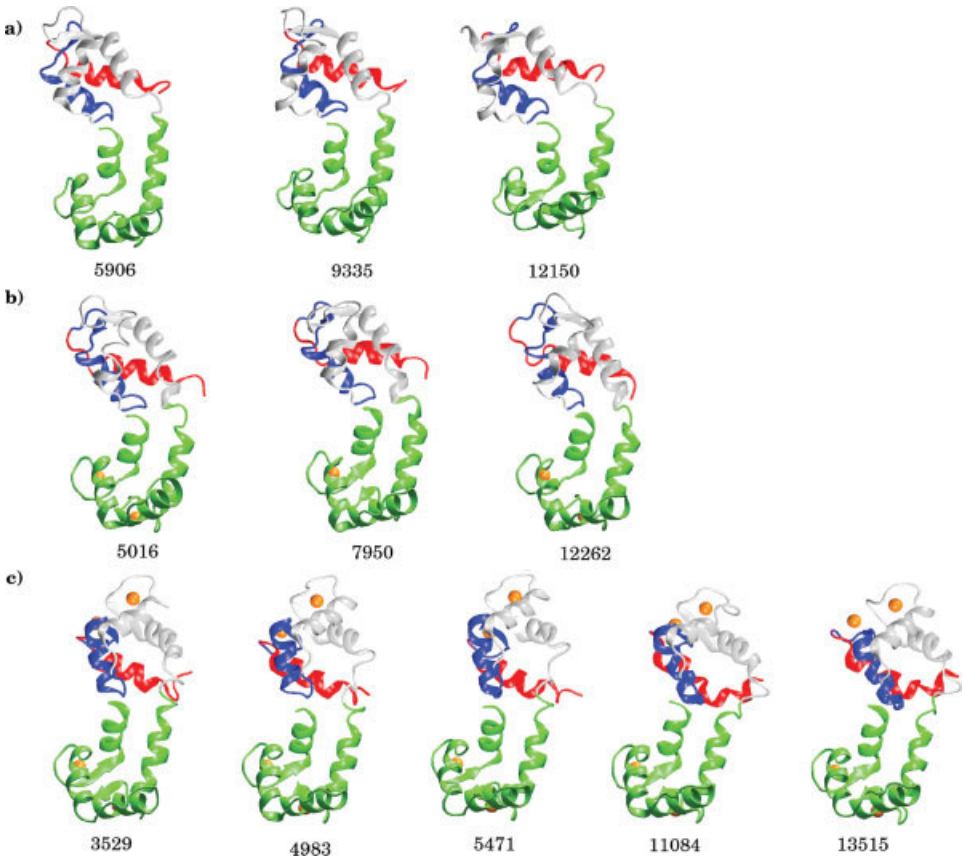

Figure 3

*Comparison of reference conformations from the (**a**) EF–(Apo-CaM), (**b**) EF–(2Ca-CaM), and (**c**) EF–(4Ca-CaM) trajectories. Calcium ions are colored in orange. Helix I of site 1 (residues 5–22), helix II of site 1 (residues 23–42), and helices V to VIII (residues 80–147) are shown in red, blue, and green, respectively. They correspond to the blocks defined in Table IX.*

tally observed for the EF-CaM complex with 2 Ca^{2+} ions.

The relative stability of the different complexes was then analyzed through the essential dynamics (ED)[66] of the two partners.

The three first modes calculated for calmodulin only contribute 61%, 58%, and 63% to the total CaM backbone mean-square fluctuations in EF–(Apo-CaM), EF–(2Ca-CaM), and EF–(4Ca-CaM), respectively. These are smaller than the 88% and 71% contributions calculated by Yang *et al.*[31] for apo and calcium-loaded forms, respectively, on MD simulations of free CaM. As expected, CaM in complex with EF undergoes less collective motions than free CaM. Eigenvalues rapidly drop in EF–(Apo-CaM) and EF–(4Ca-CaM), while EF–(2Ca-CaM) profile is smoother [Fig. 4(a)]. This suggests that motions are even less collective in EF–(2Ca-CaM) than in the two other forms: while CaM fluctuates around a stable position in EF–(2Ca-CaM), the protein evolves toward new conformations in EF–(Apo-CaM) and EF–(4Ca-CaM).

The two extreme backbone conformations of calmodulin along the first mode are displayed on Figure 5, together with the components of the mode on each atom. Deformations within the N-terminal domain are observed in the three complexes and movement of the N-tail is particularly visible in EF–(2Ca-CaM). Deformations of the interlinker region are observed in EF–(4Ca-

Table III

Coefficients c_1 and τ_1 of the Best Fitted Exponential Curves to the Average Time Autocorrelation Functions of EF–(Apo-CaM), EF–(2Ca-CaM), and EF–(4Ca-CaM)

	EF–(Apo-CaM)	EF–(2Ca-CaM)	EF–(4Ca-CaM)
c_1	0.37	0.39	0.27
τ_1	45.9	59.8	139.1

Correlations between the empirical functions and the fitted curves are within the 0.98–0.99 range.

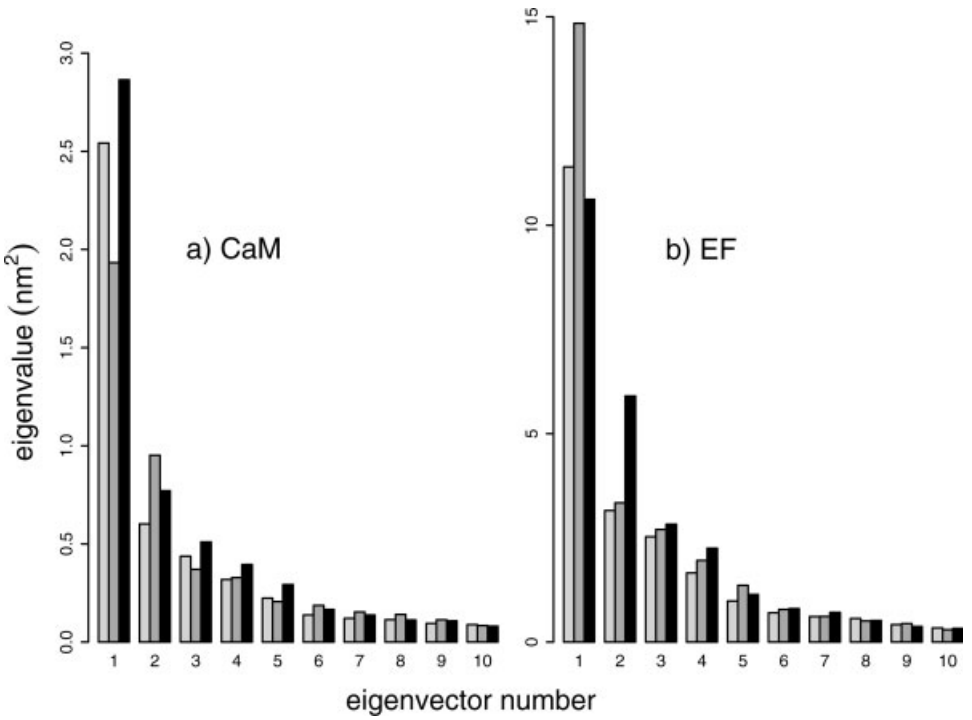

Figure 4

Eigenvalues obtained from the ED analysis performed on CaM (left) and EF (right), between 3 and 15 ns: EF–(Apo-CaM) is in lightgray, EF–(2Ca-CaM) in darkgray, and EF–(4Ca-CaM) in black.

CaM) and to a lesser extent in EF–(Apo-CaM). In EF–(Apo-CaM), both lobes tend to get closer to each other (up and down arrows) while the interlinker is pushed away (right arrows): this motion could explain the increase in global RMSD at the end of the simulation [see Fig. 1(a)].

Hence, the analysis of the collective motions of CaM reveals larger ones for EF–(Apo-CaM) and EF–(4Ca-CaM), which are experimentally unstable complexes. It is interesting to note that, in these two trajectories, the first mode involves a deformation of the interlinker domain.

In the ED analysis[66] of EF (Fig. 4), the first eigenvalue for EF–(2Ca-CaM) is the largest one [Fig. 4(b)], eigenvalues then rapidly drop and 19 modes are sufficient to describe 90% of the total fluctuations. On the other hand, 21 modes are necessary to explain 90% of the total fluctuations in EF–(4Ca-CaM) and three more are needed in EF–(Apo-CaM). Thus, motions appear to be more diffuse in these two complexes than in EF–(2Ca-CaM).

In EF–(2Ca-CaM) and in EF–(4Ca-CaM), the two first modes describe respectively a compaction [Fig. 6(a)] and a torsion [Fig. 6(b)]. Indeed, the helical domain and the CB domain move closer to each other along the x axis in the first mode, while they rotate relatively to each other around the x axis in the second mode. By contrast, the two first modes of EF in EF–(Apo-CaM) describe deformations taking place in the most flexible regions, namely the catalytic site, loops in the helical domain and switch A.

These results suggest that EF motions are more collective in EF–(2Ca-CaM) than in the other complexes, which is the contrary of what was observed for CaM. The following interpretation can then be drawn: when the complex is stable, $2Ca^{2+}$-CaM makes extensive contacts with EF and its mobility is reduced; destabilization of the EF-CaM interaction upon calcium binding or removal allows CaM to move independently from EF, in a more collective way. EF adopts the opposite behavior: as the complex is stable with two Ca^{2+}, EF has the freedom to fluctuate around an equilibrium position through global motions of the helical domain and the catalytic core; while the complex is destabilized (EF–(Apo-CaM) and EF–(4Ca-CaM)), EF mobility appears constrained and it tends to display more local motions inside its flexible regions.

Calmodulin flexibility, calcium affinity, and domain coupling in calmodulin

Atomic fluctuations per residue were calculated for CaM [Fig. 7(a,b)] as well as for EF [Fig. 7(c)] with the

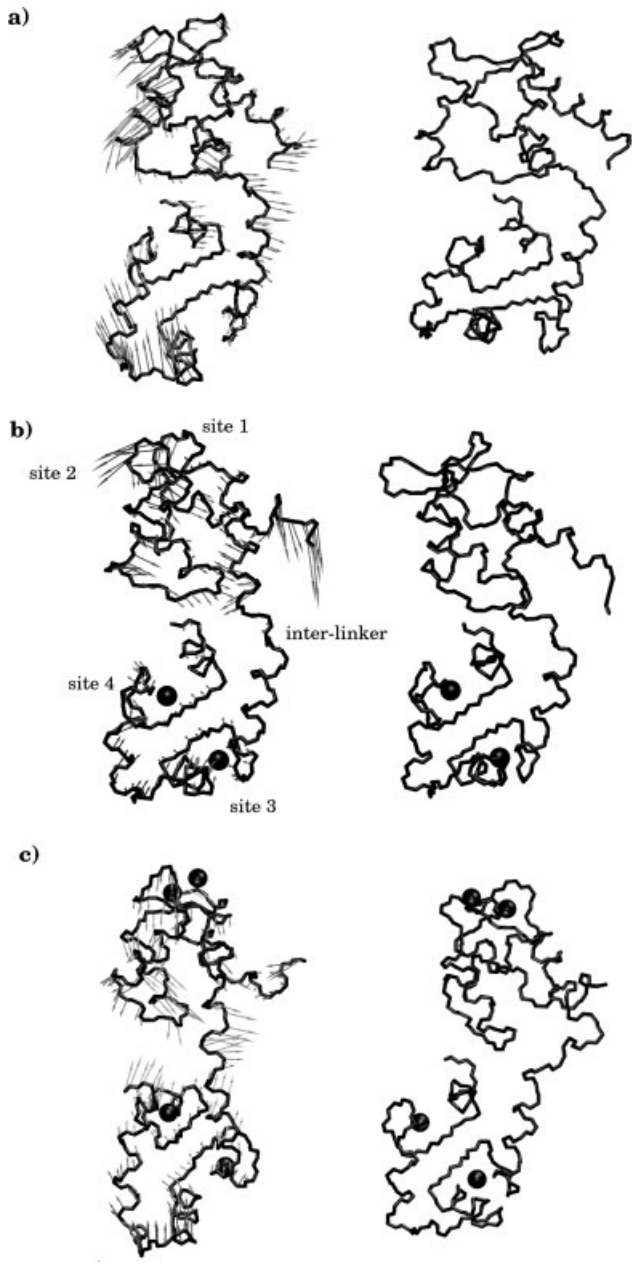

Figure 5

*Extreme conformations obtained by deforming the mean backbone conformation of CaM in (**a**) EF–(Apo-CaM), (**b**) EF–(2Ca-CaM), and (**c**) EF–(4Ca-CaM) along the first mode. On the left is represented the "starting" structure with gray arrows displaying the components of the first mode on each atom. On the right is represented the "final" structure obtained by moving along the first mode. (a) In EF–(Apo-CaM), the first mode describes deformations of site 2 (residues 45–59) within the N-terminal domain, of the region between helices VI and VII (residues 108–119) within the C-terminal domain, and of the interlinker (residues 74–80). (b) In EF–(2Ca-CaM), the first mode describes deformations of the N-terminal tail (residues 5–9) and site 2 (residues 44–60) within the N-terminal domain. (c) In EF–(4Ca-CaM), the first mode describes deformations of site 1 (residues 21–40) in the N-terminal domain, of the interlinker (residues 74–79), and locally within the C-terminal domain (residues 113–115 and 146–147).*

different levels of calcium. Changes were small for EF and will not be further described. In CaM, the N-terminal lobe (residues 5–64) interacts weakly with EF[32,42] and is flexible, in agreement with its larger RMSD [Fig. 1(c)]. Site 2 rigidifies after binding a calcium ion in EF–(4Ca-CaM) while the region upstream (residues 29–47) becomes flexible as a counterbalancing effect. By contrast site 1 coordination loop (residues 16–29) slightly gets more flexible when the level of calcium increases. The interlinker region also shows some flexibility, especially for EF–(4Ca-CaM). Although the C-terminal lobe (residues 93–147) makes extensive contacts with EF, the loop connecting the two EF-hands (residues 111–118) displays atomic fluctuations above 1.5 Å, and these fluctuations increase in the apo form.

NMR studies of CaM recently revealed that CaM internal dynamics is affected by peptide binding and highlighted the importance of conformational entropy in target recognition.[67] The crucial role of side-chains dynamics changes was illustrated in the smMLCKp-CaM and CaMKKαp-CaM complexes.[10,13] To decide whether such changes can be found in EF-bound CaM, fluctuations upon calcium binding or removal were analyzed along the simulations [Fig. 7(b)]. Overall side-chains and backbone fluctuations show similar profiles and changes according to calcium level are of small magnitude: CaM side-chains dynamics is not especially important in the EF-CaM interaction. Nevertheless, the increasing mobility of the N-terminal domain in EF–(4Ca-CaM) and of the C-terminal domain in EF–(Apo-CaM) could indicate an conformational entropic compensation for the loss of affinity of CaM for EF.

In free-CaM, calcium binding provokes the opening of the helix-loop-helix EF-hands.[19,29,30] Interhelices angles increase from 42–52° in Apo-CaM[29] to 70–95° in Ca^{2+}-CaM.[15,16] This exposes an ensemble of hydrophobic residues to solvent, which can then interact with target peptides.[31]

In the simulations of EF-CaM, both C-terminal EF-hands (sites 3 and 4) are open irrespective to the level of calcium, with interhelices angles ranging from 71.0 to 105.6° (Table IV). On the other hand, conformations of the N-terminal EF-hands (sites 1 and 2) vary upon calcium binding or removal (Table IV). Overall site 2 shows a greater variability than the other sites, as Shepherd and Vogel[19] showed in their 20-ns simulation of free Ca^{2+}-CaM. It fluctuates between a closed and a semi-open conformation in EF–(Apo-CaM) and EF–(2Ca-CaM), and slightly opens upon calcium binding in EF–(4Ca-CaM), switching between a semi-open and an open conformation.

The exposition of hydrophobic patches (defined by Yang *et al.*[31]) was evaluated (Table V) by calculating their solvent accessible surface area (SASA). In agreement with the X-ray structures 1K93, 1XFX, and 1XFY, SASA

Figure 6

*Extreme conformations obtained by deforming the mean backbone conformation of EF in EF–(2Ca-CaM) along (**a**) the first mode and (**b**) the second mode. On the left is represented the "starting" structure with gray arrows displaying the components of the first mode on each atom. On the right is represented the "final" structure obtained by moving along the first mode.*

values in the C-terminal domain are close to those of free Ca^{2+}-loaded CaM[16] (PDB entry: 1CLL), whereas SASA values in the N-terminal domain are close to those of free Apo-CaM[68] (PDB entry: 1CFD), suggesting that the formation of the EF-CaM complex selects the apo N-terminal and the Ca^{2+}-loaded C-terminal conformations, leading as expected to EF–(2Ca-CaM) as the most stable complex. Upon calcium binding, however, the N-terminal domain shows a significant gain in exposure of 12%, consistent with the opening of site 2.

Each calcium is coordinated by residues 1, 3, 5, 7, and 12 in the sequence of the interhelical loop of each EF-hand. The coordination and its electrostatic energies were analyzed (Fig. 8 and Table VI). The electrostatic binding energy ΔE_{ele} was calculated from the Coulombic interaction of calcium with the coordination loop, and is certainly a crude approximation of the experimental binding affinity. But, ΔE_{ele} gives an overall estimation of calcium coordination and allows therefore a sensitive comparison of the different sites.

Figure 8(a) displays the percentage of the simulation time spent with a given number of oxygens coordinating the Ca^{2+} ion in each EF-hand. C-terminal calcium ions (sites 3 and 4) are fully coordinated during 71% and 65% of EF–(2Ca-CaM) simulation time and are always coordinated by at least four oxygens. This proves the stability of the sites. Electrostatic binding energy (Table VI) of site 4 is significantly higher than that of site 3, in agreement with Ulmer *et al.*[43] finding on affinity.

Coordination percentages [Fig. 8(a)] and electrostatic binding energies (Table VI) in EF–(4Ca-CaM) do not significantly change for sites 3 and 4, suggesting that the stability of these sites is not altered by calcium binding on sites 1 and 2. This confirms the hypothesis of Ulmer *et al.*[43] that binding calcium on N-CaM does not affect C-CaM affinity for calcium.

By contrast, sites 1 and 2 in the N terminal domain are incompletely coordinated. Most of the time (84%), site 1 makes only 3 coordinations out of 6. Coordination in site 2 is slighlty higher, involving four or five oxygens during 35% and 59% of the time respectively. This is consistent with the stiffness observed in site 2 but not in site 1 upon calcium binding [Fig. 7(a)], and with the

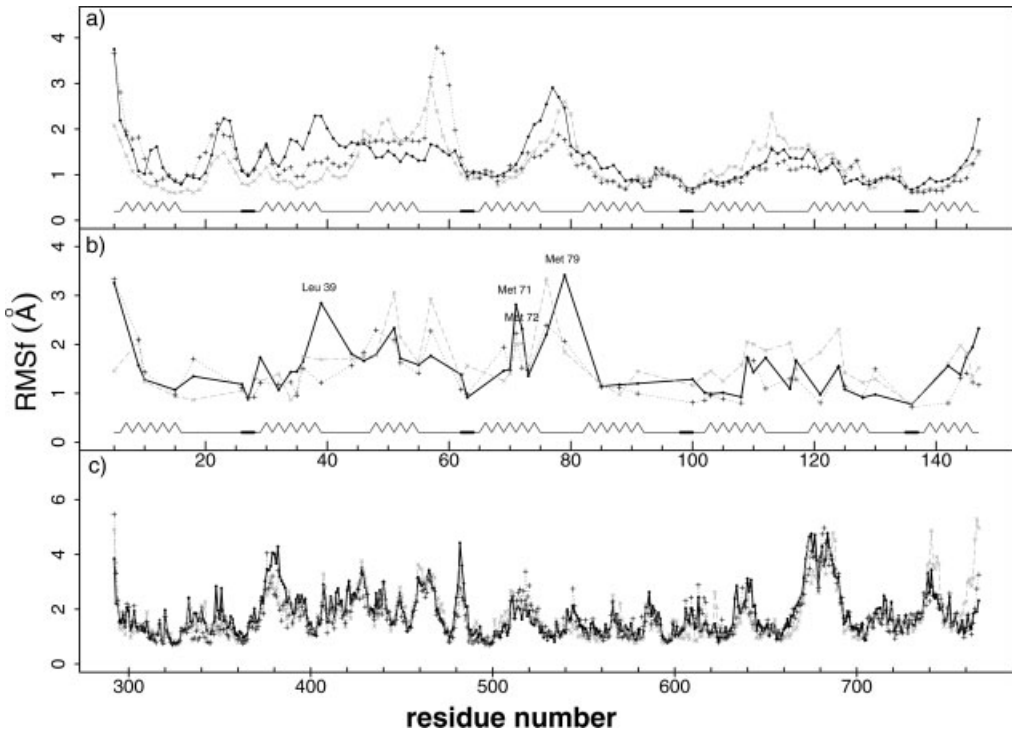

Figure 7

*Fluctuations per residue considering the last 12 ns of the EF-CaM simulations: (**a,b**) all-atoms and methyl-bearing side-chains fluctuations of calmodulin–the secondary structure is displayed at the bottom, (**c**) EF atomic fluctuations. The EF–(Apo-CaM) trajectory is shown in grey (long dotted line), the EF–(2Ca-CaM) and EF–(4Ca-CaM) trajectories are shown in black (short dotted line and solid line, respectively).*

more favorable electrostatic binding energy of Ca^{2+} in site 2 than in site 1 (Table VI).

Missing coordinating ligands can be identified in Figures 8(b,c). Glu 31 (black and grey) and Thr 26 (purple) are observed too far to participate in the coordination of site 1 [Fig. 8(b)], as described by Shen *et al.*[42] on the crystallographic structure of EF–(4Ca-CaM). In site 2 [Fig. 8(c)], Asn 60 (dark green) stays away from the Ca^{2+}, as in Shen *et al.*[42] crystallographic structure of EF–(4Ca-CaM). However, these authors found that Glu 67 did not coordinate Ca^{2+} in site 2, while both side-chains carbonyl oxygens of Glu 67 are close to the calcium ion in the simulations, around 2.7 ± 0.2 Å [Fig. 8(c)]. The affinity of N-CaM for calcium[42,43] is reduced by EF locking the domain in a closed conformation and preventing both sites 1 and 2 to fully bind calcium. This is in total agreement with SASA and EF-hand opening.

To test whether $4Ca^{2+}$-CaM could pursue toward full opening of the EF-hands when released from EF, the protein was simulated during 15 ns after removal of EF from the EF–(4Ca-CaM) crystallographic structure[42] (PDB entry: 1XFX). Mean RMS deviation on the 3–15 ns inter-

Table IV

Average Interhelical Angles in Calcium sites 1, 2, 3, and 4

	Site 1 (°)	Site 2 (°)	Site 3 (°)	Site 4 (°)
EF–(2Ca-CaM) 1K93	45.5 ± 0.2	56.3 ± 0.0	78.1 ± 0.1	88.3 ± 0.8
EF–(2Ca-CaM) 1XFY	45.3 ± 0.0	53.8 ± 0.0	75.4 ± 0.0	83.2 ± 0.0
EF–(4Ca-CaM) 1XFX	45.8 ± 0.0	58.8 ± 0.2	76.4 ± 0.0	83.0 ± 0.0
EF–(Apo-CaM) MD	33.4 ± 3.9	62.6 ± 8.5	79.8 ± 3.8	94.8 ± 4.3
EF–(2Ca-CaM) MD	41.2 ± 2.3	60.2 ± 7.3	74.4 ± 3.4	98.3 ± 3.8
EF–(4Ca-CaM) MD	43.7 ± 7.2	75.7 ± 7.7	80.4 ± 2.7	101.0 ± 4.6

These angles describe the opening of EF hands.

Table V
Solvent Accesible Surface Area (SASA, Å^2) Calculated on the Hydrophobic Patches of the N-Terminal and C-Terminal Domains of Calmodulin

	No calcium		Two calcium ions		Four calcium ions	
	N-term	C-term	N-term	C-term	N-term	C-term
Free CaM (X-ray)[16,68]	406	490	—		694	784
EF-bound CaM (X-ray)[32]	—		641	784	—	
EF-bound CaM (X-ray)[42]	—		468	733	527	766
EF-bound CaM (MD)	443 ± 45	810 ± 38	476 ± 68	835 ± 32	505 ± 42	840 ± 31

Values are calculated on (i) free CaM and on (ii) CaM in complex with EF. Free CaM values are calculated on the 1CDL X-Ray structure of free Apo-CaM[68] and on the 1CLL X-Ray structure of free Ca^{2+}-loaded CaM.[16] EF-bound CaM values are calculated on the X-Ray structures of the EF-CaM complex – the 1K93 structure of EF–(2Ca-CaM),[32] and the 1XFY and 1XFX structures of EF–(2Ca-CaM) and EF–(4Ca-CaM),[42] and on the EF–(Apo-CaM), EF–(2Ca-CaM) and EF–(4Ca-CaM) MD trajectories.

val is 7.8 Å. Contrary to what was expected, the simulation did not converge toward the opening of the N-terminal domain. Interhelical angles were rather stable around 40° ± 3° in site 1, 47° ± 5° in site 2, 84° ± 10° in site 3, and 76° ± 3° in site 4. SASA of the hydrophobic patches was about 400 Å^2 in N-CaM and 800 Å^2 in C-CaM. An essential dynamics (ED) analysis allowed to observe a reorientation of the lobes relative to each other (Fig. 9). It appears thus easier for the released 4Ca-CaM to reorientate its lobes than to open its N-terminal domain. This observation agrees with the structure of the free 4Ca^{2+}-CaM recently solved by Grabarek,[71] where N-CaM is artificially locked in a closed conformation by a disulfide bond, revealing a two-step calcium binding mechanism. The structure of 4Ca-CaM in the EF–(4Ca-CaM) complex is also intermediate between the closed and open conformations, lacking the final Glu 12 ligand in the N-terminal coordination loops. This state corresponds to the first step of dissociation observed in a steered MD.[72]

Mechanical model of the CaM-EF interaction

A mechanical model of the CaM-EF interaction was derived from the analyses of (i) calmodulin conformation and (ii) the EF-CaM interaction.

The average CaM radii of gyration [Fig. 10(a)] during the simulations range from 18.6 to 19.6 Å with standard deviations of 0.3 Å. These values reveal an intermediate conformation between the extended conformation of Ca^{2+}-CaM in crystal (21.9 Å)[16] and the compact conformation of smMLCK peptide-bound CaM (16.1 Å).[17]

In EF–(Apo-CaM) and EF–(2Ca-CaM), CaM tends to become more compact during the trajectories than in the crystalline environment[32,42] (Table VII). In EF–(4Ca-CaM) however, CaM average radius of gyration is slightly

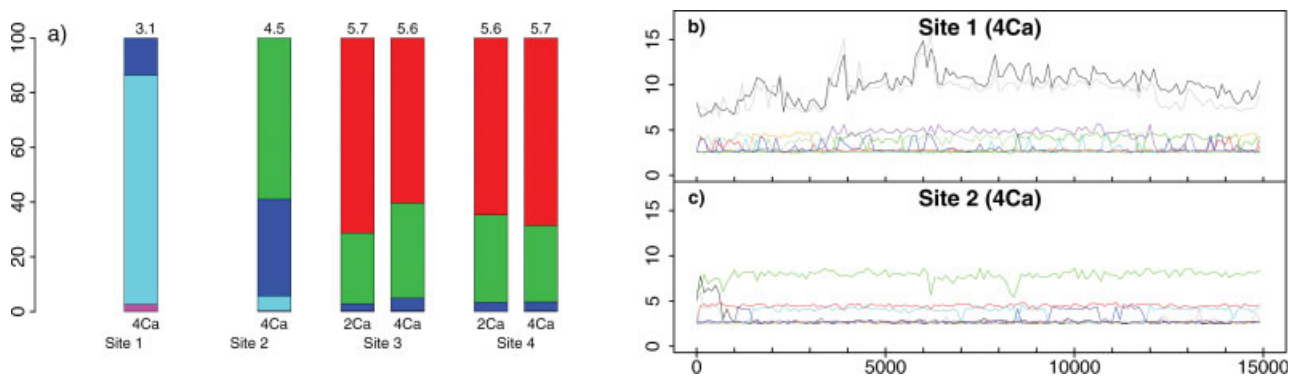

Figure 8
*Calcium coordination in (**b,c**) sites 1 and 2 of EF–(4Ca-CaM), (**a**) sites 1–4 of EF–(2Ca-CaM) and EF–(4Ca-CaM). (a) Each colour stands for a level of calcium coordination: 2 oxygens in purple, 3 oxygens in light blue, 4 oxygens in dark blue, 5 oxygens in green, and full coordination with 6 oxygens in red. At the top is written the mean coordination level. Oxygens are considered to coordinate the calcium ion if they are located at less than 2.8 Å from it, consistent with typical calcium coordination distances found in the literature.[69,70] (b,c) Coordination distances in (b) site 1 and (c) site 2 along the EF–(4Ca-CaM) trajectory. In site 1, coordination distances are calculated between the calcium ion and D20.Oδ1 (red), D20.Oδ2 (orange), D22.Oδ1 (dark blue), D22.Oδ2 (light blue), D24.Oδ1 (dark green), D24.Oδ2 (light green), T26.0 (purple), E31.Oε1 (black), and E31.Oε2 (grey). In site 2, coordination distances are calculated between the calcium ion and D56.Oδ1 (red), D56.Oδ2 (orange), D58.Oδ1 (dark blue), D58.Oδ2 (light blue), N60.Oδ1 (dark green), T62.0 (purple), E67.Oε1 (black), and E67.Oε2 (grey).*

Table VI
Electrostatic Binding Energies ΔE_{ele} of Calcium Ions in Each Site of EF–(2Ca-CaM) and EF–(4Ca-CaM), in kcal mol^{-1}

	Site 1	Site 2	Site 3	Site 4
EF–(2Ca-CaM)	—	—	−1245 ± 102	−1444 ± 102
EF–(4Ca-CaM)	−1160 ± 100	−1294 ± 100	−1265 ± 100	−1475 ± 100

larger, of 19.6 ± 0.4 Å. Indeed, as described in a previous section, the N-terminal domain slightly opens upon calcium binding in EF–(4Ca-CaM).

The VDA formed by the EF-hands centres of mass characterizes the relative orientation of the lobes [Fig. 10(b)]. CaM adopts an acute or right VDA (between −100 and −60°) during the simulations, as in other target-CaM complexes,[17] whereas free CaM displays an obtuse VDA.[16,18–20] For EF–(4Ca-CaM) and EF–(Apo-CaM), the VDA was around −70° and −94°, respectively, while it fluctuates between the two other profiles around −84° for EF–(2Ca-CaM). Thus, binding (respectively removing) two calcium ions stabilizes the orientation of CaM lobes, toward a smaller (respectively larger) VDA value.

To characterize the behavior of the interlinker region, its secondary structure was determined using DSSP[58] and averaged over the whole simulations [Fig. 10(d)]. The percentages of simulation time spent in helical secondary structure, hydrogen bonded turn, or random coil are given for each residue. EF–(2Ca-CaM) displays the highest average helical content (74.6%), consistent with the stability of the RMSD (Fig. 1).

The central region of the interlinker lacks of helical secondary structure: the nonhelical structures extends from residues 73 to 82 in EF–(Apo-CaM), 71 to 84 in EF–(2Ca-CaM), and 69 to 84 in EF–(4Ca-CaM). These residues switch from helix to turn or random coil in different proportions according to the level of calcium. Removing two calcium ions from the C-terminal domain provokes a partial unfolding of the interlinker (residues 76–78) in EF–(Apo-CaM) whereas binding two calcium ions on the N-terminal domain provokes a partial transition to turn (residues 73–82) in EF–(4Ca-CaM).

We evaluated the bending of the interlinker as the angle between helices IV and V [Fig. 10(c)]. While the angle of EF–(Apo-CaM) and EF–(2Ca-CaM) stays stable around 132° and 126°, it stabilizes around 109° for EF–(4Ca-CaM). This more pronounced bending might be the result of the conversion of the helical secondary structures to turns, with a hinge formed by the central residues.

Previous MD simulations of free Ca^{2+}-loaded CaM also showed a loss of helical structure in the interlinker[18,19,65] associated with the bending. Moreover, Shepherd and Vogel[19] found in their 20-ns simulation that partial unfolding of residues 75–81 participated in the bending of the interlinker and in the associated compaction event of CaM. We do not observe such a compaction as the bending is not sufficient to counter-balance the expansion of the N-terminal domain in EF–(4Ca-CaM).

It was observed in the literature[19,20] that the bending or unwinding of the interlinker region is loosely stabilized by some hydrogen bonds formed between central residues and the N-terminus. Although CaM sequence in the EF-CaM complex lacks residues 1–4, we found similar stabilizing interactions in EF–(Apo-CaM) as well as in EF–(4Ca-CaM), but not in EF–(2Ca-CaM), consistent with the greater flexibility of CaM N-tail in this complex [Fig. 7(a)]. Indeed, in EF–(Apo-CaM), hydrogen bonds T5.N-T77.O, T5.N-T79.O, T5.Hγ1-T77.O, T5.Oγ1-T79.Hγ1 appear to stabilize the unwinding of the inter-

Figure 9
First mode of the essential dynamics analysis of the simulation of 4Ca-CaM released from EF. Gray arrows display the components of the mode on each backbone atom.

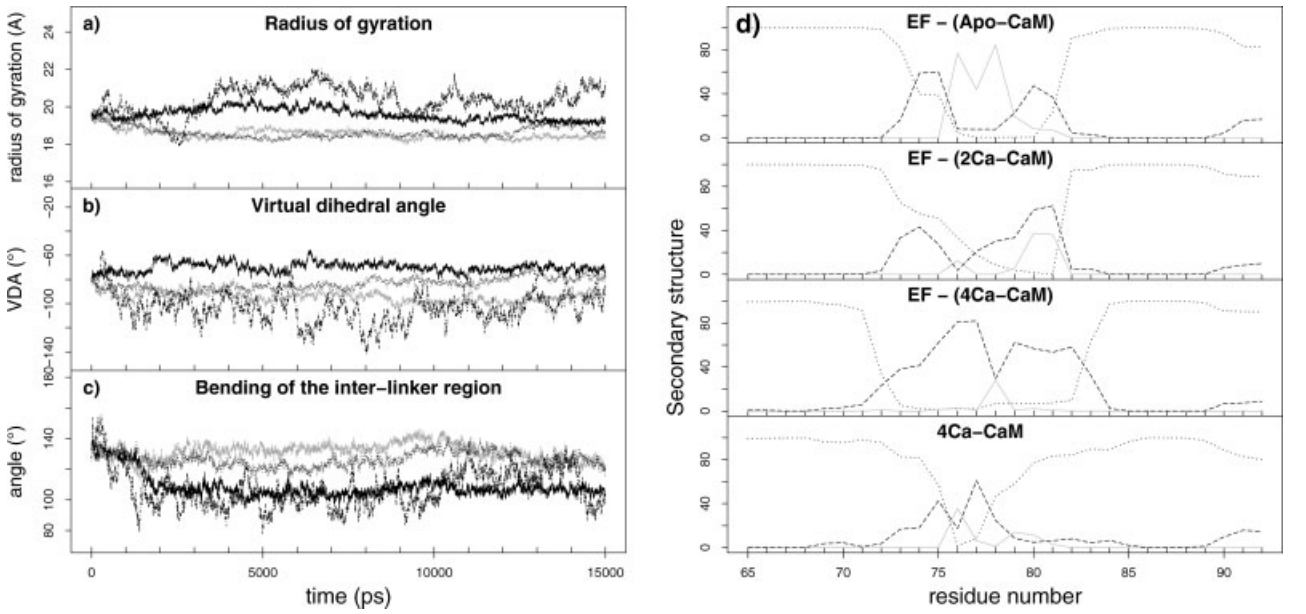

Figure 10

*(**a–c**) Radius of gyration (a), VDA (b), and bending of the interlinker (c) of calmodulin along the simulations. The EF–(Apo-CaM) trajectory is shown in gray (long dotted line), the EF–(2Ca-CaM) and EF–(4Ca-CaM) trajectories are shown in black (dotted and thick line, respectively), the 4Ca-CaM trajectory is shown in black (dotted and long dashed line). (d) Secondary structure averaged over the whole simulations. The percentage of simulation time spent by each residue in each secondary structure type is given. The black short dotted, black long dotted, and grey solid lines represent the helical, turn, and random coil types, respectively.*

linker. In EF–(4Ca-CaM), the Q8.Oε1-T79.Hγ1 hydrogen bond, formed in the 8–15 ns interval, and hydrophobic interactions between N-terminus and interlinker residues participate in the bending of the interlinker.

Therefore, analysis of the radius of gyration, of the VDA, of the bending of the interlinker, and the of interactions within CaM show that CaM conformations in EF-(Apo-CaM) and EF-(2Ca-CaM) are similar whereas that in EF-(4Ca-CaM) is significantly different. One should notice that EF-(2Ca-CaM) and EF-(4Ca-CaM) conformations in crystal were quite similar, and that MD trajectories allow further exploration of the conformational space.

The analysis of EF conformation in the EF-CaM complex reveals a calcium-dependent behavior different from that of CaM. Adding two calcium ions to EF–(2Ca-CaM) has little effect on EF conformation, whereas removing two calcium ions affects the whole protein, and especially the geometry of the catalytic site. As showed in Figure 11(a,b), the time evolution of some characteristic distances between the centres of mass of EF domains are similar for EF–(2Ca-CaM) and EF–(4Ca-CaM) but are often significantly different for EF–(Apo-CaM). Opening of the EF catalytic site was monitored through the mean distance between the centres of mass of residues from Switch B (H577, G578, T579, D582, N583, E588, F586) and residues from CB (H351, K353, S354, K372) (Table VIII). Indeed, this distance has a similar evolution, in the 13–15 Å range, for EF–(2Ca-CaM) and EF–(4Ca-CaM), while it decreases slightly, around 11.3 Å for EF–(Apo-CaM). N329, K353,

Table VII

Conformational Parameters of CaM (Radius of Gyration, Virtual Dihedral Angle (VDA), and Bending of the Interlinker Region) Calculated on EF-CaM X-ray Structures[32,42] and on MD Trajectories

		Radius of gyration (Å)	VDA (°)	Bending (°)
X-ray PDB	EF–(2Ca-CaM)(1K93)[32]	19.5	−80.5	124
	EF–(2Ca-CaM)(1XFY)[42]	19.2	−76.9	125
	EF–(4Ca-CaM)(1XFX)[42]	19.4	−77.3	120
MD trajectories	EF–(Apo-CaM)	18.5 ± 0.2	−95.2 ± 3.8	132 ± 5
	EF–(2Ca-CaM)	18.5 ± 0.2	−82.7 ± 4.6	126 ± 5
	EF–(4Ca-CaM)	19.6 ± 0.4	−69.8 ± 3.7	106 ± 4

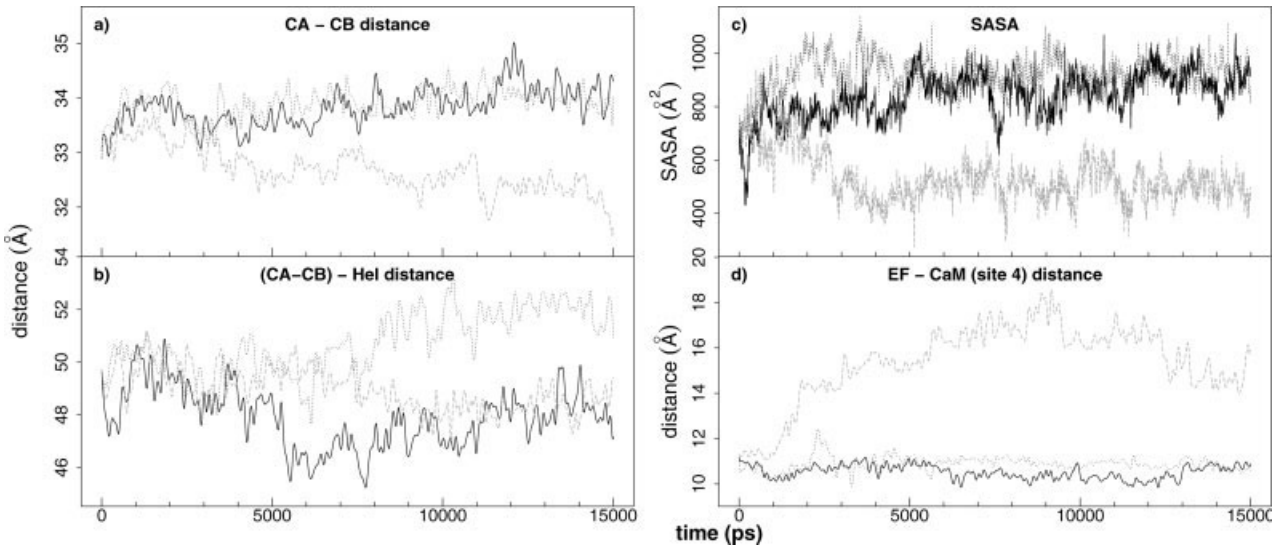

Figure 11

*Characteristic features of EF conformations along the trajectories: (**a**) distance between the centers of mass of CA (residues 292 to 349 and 490 to 622) and CB (residues 350 to 489), (**b**) distance between the centers of mass of the catalytic core (grouping CA and CB) and Hel (residues 660 to 767), (**c**) SASA of the catalytic site (H351, K353, S354, K372, R329, K346, L348, D491, D493, H577, G578, T579, D582, N583, E588, F586, T548), (**d**) distance between the center of mass of EF C-tail (residues 758 to 767) and the center of mass of the coordinating ligands in site 4 of CaM.*

K346 establish hydrogen bonds with the ligand in Shen *et al.*[42] and the triangle distances between these residues (Table VIII) is thus also indicative of the opening of EF catalytic site during the trajectories. In EF–(Apo-CaM) N329.Cγ is closer to K353.Nζ and to K346.Nζ, than in the other two trajectories. Calculations of the accessible surface area (SASA) in the catalytic site also support [Fig. 11(c), Table VIII] the hypothesis of the active site collapse in EF-(Apo-CaM). The SASA values calculated from the simulations of EF–(2Ca-CaM) and EF–(4Ca-CaM) are slightly larger, but in qualitative agreement with the X-ray structures 1XFX and 1XFY of the complexes.

To characterize contacts between EF and CaM in the complex, hydrophobic interactions and hydrogen bonds established for at least 50% of the simulation time were analyzed (Table IX). The C-terminal domain of calmodulin makes extensive contacts with EF: an average of 40 C-terminal residues are involved in either hydrophobic interactions or hydrogen bonds, whereas there are only about five N-terminal residues interacting with EF (Table IX). In the N-terminal domain, the hydrogen bonds form the majority of contacts for EF–(2Ca-CaM), whereas they are a minority for EF–(Apo-CaM) and EF–(4Ca-CaM). The changes observed in the N-terminal

Table VIII

Average Characteristic Distances and Solvent Accessible Surface (SASA) Within EF Catalytic Site Including the Residues (H351, K353, S354, K372, R329, K346, L348, D491, D493, H577, G578, T579, D582, N583, E588, F586, T548)

	SB-CB (Å)	N329.Cγ K353.Nζ (Å)	N329.Cγ-K346.Nζ (Å)	SASA (Å^2)
Apo-EF 1K8T[32]	—	11.3	12.2	786
EF–(2Ca-CaM) 1K93[32]	13.6	7.5	9.6	703
EF–(2Ca-CaM) 1XFY[42]	15.1	11.1	10.1	833
EF–(4Ca-CaM) 1XFX[42]	15.2	11.2	10.3	827
EF–(Apo-CaM) MD	11.3 ± 0.5	6.4 ± 0.8	11.0 ± 1.0	501 ± 58
EF–(2Ca-CaM) MD	14.4 ± 1.1	11.1 ± 1.8	13.1 ± 1.2	928 ± 55
EF–(4Ca-CaM) MD	13.7 ± 0.9	11.4 ± 1.9	13.7 ± 1.6	866 ± 70

The SB-CB distance is calculated between the centers-of-mass of residues H577, G578, T579, D582, N583, E588, and F586 from SB and residues H351, K353, S354, and K372 from CB. Residues N329, K346, K353 were chosen as they establish in the X-ray structure[42] a network of hydrogen bonds.

Table IX
Number of CaM Residues that Are Involved in Hydrogen Bonds with EF/ Number of CaM Residues that Are Involved in Hydrophobic Interactions with EF (for at least 50% of the Simulation Time)

	EF–(Apo-CaM)	EF–(2Ca-CaM)	EF–(4Ca-CaM)
Helix I	4/6	4/3	3/6
Helix II	2/4	1/1	0/2
C-term	12/28	15/29	16/28

Residues are grouped by blocks: Helix I comprises helix I of site 1 (residues 5–22), Helix II comprises helix II of site 1 (residues 23–42), C-term comprises helices V to VIII (residues 80–147).

domain agree with the conformational variability of the reference structures (Fig. 3) in the convergence analysis. The balance between hydrogen bonds and hydrophobic contacts may thus be related to the specificity of the EF-CaM interaction.

In the crystallographic structures of EF-CaM with 2 and 4 Ca^{2+},[32,42] a key salt bridge was formed between Asp 647 from the switch C of EF and Arg 90 from the interlinker of CaM. Two salt bonds between Oδ2 of Asp 647 and the Nε and Nη2 of Arg 90 are stable along the EF–(2Ca-CaM) as well as the EF–(Apo-CaM) trajectories. In EF–(4Ca-CaM), side-chains of the two residues rapidly moved away from each other, but both salt bonds are formed again around 12 ns up to the end of the trajectory.

Figure 11(d) reveals that the removal of calcium from C-CaM in EF–(Apo-CaM) allows EF C-tail to move away from site 4 (11.1 Å at $t = 0$ and around 16.0 Å in the 3–15 ns interval). On the contrary, the distance stays stable, around 10.5 Å for EF–(2Ca-CaM) and EF–(4Ca-CaM).

CONCLUSION

In this study, we focused on the conformational plasticity of CaM in the EF-CaM complex and we evaluated the impact of calcium binding or removal on the stability of the complex. We performed three 15-ns MD simulations of the EF-CaM complex corresponding to three different levels of calcium. Such simulations exhibit a much longer time period and more accurate conditions (periodic boundaries, PME) than the early 350-ps simulations of EF–(2Ca-CaM).[46] Values of radius of gyration, VDA, EF-hands opening, and hydrophobic patches calculated on the EF–(2Ca-CaM) and EF–(4Ca-CaM) trajectories were found in good agreement with measurements on the corresponding experimental X-ray structures.[32,42] The EF-(2Ca-CaM) trajectory displays the most stable features (convergence, calcium coordination, essential dynamics), in agreement with experiments.

The trajectories presented here have been validated through their comparison with X-ray crystallographic structures. They can consequently be used: (i) to draw a more dynamical picture of the EF-(2Ca-CaM) and EF-(4Ca-CaM) complexes, (ii) to give reasons for the experimental instability of the EF-(Apo-CaM) complex.

The most striking dynamics feature is the role played by the bending motion of CaM interlinker. Indeed, fluctuations of EF-bound CaM are mostly the result of deformations inside the N-terminal domain and bending of the interlinker region. This motion is important for the fitting of the size of CaM to the distance between EF helical and CB domains. In EF–(4Ca-CaM), calcium binding provokes the expansion of the N-terminal domain and the bending of the interlinker, from 126 down to 109°. The exposure of hydrophobic patches promotes contacts between the interlinker region and the N-tail of CaM, which stabilizes the bending of the interlinker.

Through the bending of the interlinker, CaM plays the role of a spring which maintains EF in an open conformation, inducing the activation of the adenylyl cyclase catalytic site. The two Ca^{2+} complexation level gives the best fit to EF open conformation: indeed, EF–(Apo-CaM) and EF–(4Ca-CaM) both display a deformation of the interlinker.

The N- and C-terminal lobes of CaM are locked by EF in configurations similar to closed-like and open-like conformations, whatever the level of calcium complexation. Nevertheless, limited opening of the N-terminal domain of CaM was observed in EF–(4Ca-CaM) and illustrates the general opening mechanism of CaM upon calcium binding. Site 1 only reaches the first step of calcium binding and its calcium coordination loop lacks the final Glu 12 ligand. Consequently N-CaM is trapped in an intermediate closed conformation, from which it cannot escape.

The presence of EF not only disturbs CaM affinity for calcium but also the coupling mechanism between the two CaM lobes through the interlinker region. EF allows coupling between CaM lobes, but only in one direction, that is from C-CaM to N-CaM. Indeed, binding two calcium ions on N-CaM provokes only changes in the fluctuations of both the interlinker and the N-terminal domain itself. On the other hand, removing two calcium ions from the C-CaM provokes changes in the fluctuations of the C-terminal domain itself and also in the N-terminal domain. This asymmetry in coupling is also observed in the variation of hydrophobic patches. The N-terminal hydrophobic patches of CaM gain almost the same surface (29 $Å^2$) upon calcium binding than the one they loose (33 $Å^2$) in EF–(Apo-CaM). On the other hand, the C-terminal patches gain about 5 $Å^2$ in EF–(4Ca-CaM) and loose about 25 $Å^2$ upon calcium removal. This might be a consequence of a stronger interaction between EF and C-CaM than with N-CaM.

The removal of all calciums was also studied in the present work, which gives information about the EF–(Apo-CaM) system, for which no structure has been solved to date. Ulmer *et al.*[43] proposed a model where

Apo-CaM only interacts with EF through its N-terminal domain. Indeed, we observed that the interaction between EF and the C-terminal domain of CaM is weakened in EF–(Apo-CaM).

However, our analyses of radius of gyration, VDA, opening of the sites, and exposure of hydrophobic patches showed that the conformation of CaM in EF–(Apo-CaM) is closer to that of EF–(2Ca-CaM) than that of EF–(4Ca-CaM). This suggests that once the C-terminal domain is inserted and blocked between the helical domain and the catalytic core of EF, the stability of the complex is not dramatically affected upon calcium removal. An energetic barrier opposes the formation of EF–(Apo-CaM) but there is also a symmetric energetic barrier opposing the dissociation of the complex upon removal of the C-terminal calcium ions. The results presented are mainly influenced by the second barrier.

Besides, reactions to calcium binding or removal suggest a mechanism for the destabilization of the EF–(Apo-CaM) complex. Indeed, our study suggests that the binding of calcium on N-CaM tends to open the domain, but this opening is restrained by EF helical domain, which keeps the catalytic site open and maintains its contacts with CaM site 1. On the other hand, C-CaM is deeply inserted between the catalytic core and the helical domain of EF, and cannot relax. The removal of Ca^{2+} ions from C-CaM will induce a tension toward EF, and thus explains the deformations observed in EF bound to Apo-CaM, which bring the EF domains closer and induce a collapse of the catalytic site.

The present work brings a contribution to the global knowledge of CaM conformational plasticity and describes its molecular interaction with a pathological agent. By giving clues to a better understanding of the mechanisms played in the EF-CaM complex, it enables to better characterize the CaM molecular features responsible for its regulation of many targets. It also permits to define what makes the specificity of CaM recruitment by a toxin, compared to the recognition and activation of target proteins in cellular signalling pathways.

ACKNOWLEDGMENTS

We thank the French Ministry of Defence (DGA/MRIS), the National Scientific Research Centre (CNRS) and the Pasteur Institute for fundings and support. We also acknowledge the French National Calculations Centres IDRIS (Orsay) and CINES (Montpellier) for computational resources. JY acknowledges the FAPERJ (Brazil) for an undergraduate fellowship.

REFERENCES

1. Ikura M, Ames JB. Genetic polymorphism and protein conformational plasticity in the calmodulin superfamily: two ways to promote multifunctionality. Proc Natl Acad Sci USA 2006;103:1159–1164.
2. Ikura M, Marion D, Kay LE, Shih H, Krinks M, Klee CB, Bax A. Heteronuclear 3D NMR and isotopic labeling of calmodulin. Towards the complete assignment of the ^{1}H NMR spectrum. Biochem Pharmacol 1990;40:153–160.
3. Ikura M, Kay LE, Bax A. A novel approach for sequential assignment of ^{1}H, ^{13}C, and ^{15}N spectra of proteins: heteronuclear triple-resonance three-dimensional NMR spectroscopy. Application to calmodulin. Biochemistry 1990;29:4659–4667.
4. Ikura M, Kay LE, Bax A. Improved three-dimensional ^{1}H-^{13}C-^{1}H correlation spectroscopy of a ^{13}C-labeled protein using constant-time evolution. J Biomol NMR 1991;1:299–304.
5. Bax A, Ikura M. An efficient 3D NMR technique for correlating the proton and ^{15}N backbone amide resonances with the alpha-carbon of the preceding residue in uniformly ^{15}N/^{13}C enriched proteins. J Biomol NMR 1991;1:99–104.
6. Friedrichs MS, Mueller L, Wittekind M. An automated procedure for the assignment of protein ^{1}HN, ^{15}N, ^{13}Cα, ^{1}Hα, ^{13}Cβ and ^{1}Hβ resonances. J Biomol NMR 1994;4:703–726.
7. Lee AL, Sharp KA, Kranz JK, Songn XJ, Wandn AJ. Temperature dependence of the internal dynamics of a calmodulin-peptide complex. Biochemistry 2002;41:13814–13825.
8. Petrone P, Pande VS. Can conformational change be described by only a few normal modes? Biophys J 2006;90:1583–1593.
9. Chen K, Ruan J, Kurgan LA. Prediction of three dimensional structure of calmodulin. Protein J 2006;25:57–70.
10. Frederick KK, Kranz JK, Wand AJ. Characterization of the backbone and side chain dynamics of the CaM-CaMKIp complex reveals microscopic contributions to protein conformational entropy. Biochemistry 2006;45:9841–9848.
11. Qin Z, Wertz SL, Jacob J, Savino Y, Cafiso DS. Defining protein–protein interactions using site-directed spin-labeling: the binding of protein kinase C substrates to calmodulin. Biochemistry 1996;35:13272–13276.
12. Lee AL, Kinnear SA, Wand AJ. Redistribution and loss of side chain entropy upon formation of a calmodulin-peptide complex. Nat Struct Biol 2000;7:72–77.
13. Marlow MS, Wand AJ. Conformational dynamics of calmodulin in complex with the calmodulin-dependent kinase kinase α calmodulin-binding domain. Biochemistry 2006;45:8732–8741.
14. Ishida H, Vogel HJ. Protein–peptide interaction studies demonstrate the versatility of calmodulin target protein binding. Protein Pept Lett 2006;13:455–465.
15. Babu YS, Bugg CE, Cook WJ. Structure of calmodulin refined at 2.2 Å resolution. J Mol Biol 1988;204:191–204.
16. Chattopadhyaya R, Meador WE, Means AR, Quiocho FA. Calmodulin structure refined at 1.7 Å resolution. J Mol Biol 1992;228:1177–1192.
17. Meador WE, Means AR, Quiocho FA. Target enzyme recognition by calmodulin: 2.4 Å structure of a calmodulin-peptide complex. Science 1992;257:1251–1255.
18. Wriggers W, Mehler E, Pitici F, Weinstein H, Schulten K. Structure and dynamics of calmodulin in solution. Biophys J 1998;74:1622–1639.
19. Shepherd CM, Vogel HJ. A molecular dynamics study of Ca^{2+}-calmodulin: evidence of interdomain coupling and structural collapse on the nanosecond timescale. Biophys J 2004;87:780–791.
20. Fiorin G, Biekofsky RR, Pastore A, Carloni P. Unwinding the helical linker of calcium-loaded calmodulin: a molecular dynamics study. Proteins 2005;61:829–839.
21. Chou JJ, Li S, Klee CB, Bax A. Solution structure of Ca^{2+}-calmodulin reveals flexible hand-like properties of its domains. Nat Struct Biol 2001;8:990–997.
22. Bertini I, Del Bianco C, Gelis I, Katsaros N, Luchina C, Parigi G, Peana M, Provenzani A, Zoroddu MA. Experimentally exploring the conformational space sampled by domain reorientation in calmodulin. Proc Natl Acad Sci USA 2004;101:6841–6846.
23. Johnson CK. Calmodulin, conformational states, and calcium signaling. A single-molecule perspective. Biochemistry 2006;45:14233–14246.

24. Wilson MA, Brunger AT. The 1.0 Å crystal structure of Ca(2+)-bound calmodulin: an analysis of disorder and implications for functionally relevant plasticity. J Mol Biol 2000;301:1237–1256.
25. Fallon JL, Quiocho FA. A closed compact structure of native Ca^{2+}-calmodulin. Structure 2003;11:1303–1307.
26. Gifford JL, Walsh MP, Vogel HJ. Structures and metal-ion-binding properties of the Ca^{2+}-binding helix-loop-helix EF-hand motifs. Biochem J 2007;405:199–221.
27. Capozzi F, Casadei F, Luchinat C. EF-hand protein dynamics and evolution of calcium signal transduction: an NMR view. J Biol Inorg Chem 2006;11:949–962.
28. Ishida H, Takahashi K, Nakashima K, Kumaki Y, Nakata M, Hikichi K, Yazawa M. Solution structures of the N-terminal domain of yeast calmodulin: Ca^{2+}-dependent conformational change and its functional implication. Biochemistry 2000;39:13660–13668.
29. Zhang M, Tanaka T, Ikura M. Calcium-induced conformational transition revealed by the solution structure of apo calmodulin. Nat Struct Biol 1995;2:758–767.
30. Finn BE, Evenas J, Drakenberg T, Waltho JP, Thulin E, Forsen S. Calcium-induced structural changes and domain autonomy in calmodulin. Nat Struct Biol 1995;2:777–783.
31. Yang C, Jas GS, Kuczera K. Structure, dynamics and interaction with kinase targets: computer simulations of calmodulin. Biochim Biophys Acta 2004;1697:289–300.
32. Drum CL, Yan SZ, Bard J, Shen YQ, Lu D, Soelaiman S, Grabarek Z, Bohm A, Tang WJ. Structural basis for the activation of anthrax adenylyl cyclase exotoxin by calmodulin. Nature 2002;415:396–402.
33. Elshorst B, Hennig M, Forsterling H, Diener A, Maurer M, Schulte P, Schwalbe H, Griesinger C, Krebs J, Schmid H, Vorherr T, Carafoli E. NMR solution structure of a complex of calmodulin with a binding peptide of the Ca^{2+} pump. Biochemistry 1999;38:12320–12332.
34. Schumacher MA, Rivard AF, Bachinger HP, Adelman JP. Structure of the gating domain of a Ca^{2+}-activated K^+ channel complexed with Ca^{2+}/calmodulin. Nature 2001;410:1120–1124.
35. Hoeflich KP, Ikura M. Calmodulin in action: diversity in target recognition and activation mechanisms. Cell 2002;108:739–742.
36. Vetter SW, Leclerc E. Novel aspects of calmodulin target recognition and activation. Eur J Biochem 2003;270:404–414.
37. Liddington RC. Anthrax: a molecular full nelson. Nature 2002;415: 373–374.
38. Ascenzi P, Viscaa P, Ippolitob G, Spallarossac A, Bolognesic M, Montecuccod C. Anthrax toxin: a tripartite lethal combination. FEBS Lett 2002;531:384–388.
39. Collier RJ, Young JA. Anthrax toxin. Annu Rev Cell Dev Biol 2003; 19:45–70.
40. Abrami L, Reig N, van der Goot FG. Anthrax toxin: the long and winding road that leads to the kill. Trends Microbiol 2005;13:72–78.
41. Lee YS, Bergson P, He WS, Mrksich M, Tang WJ. Discovery of a small molecule that inhibits the interaction of anthrax edema factor with its cellular activator, calmodulin. Chem Biol 2004;8:1139–1146.
42. Shen Y, Zhukovskaya NL, Guo Q, Florian J, Tang WJ. Calcium-independent calmodulin binding and two-metal-ion catalytic mechanism of anthrax edema factor. EMBO J 2005;24:929–941.
43. Ulmer TS, Soelaiman S, Li S, Klee CB, Tang WJ, Bax A. Calcium dependence of the interaction between calmodulin and anthrax edema factor. J Biol Chem 2003;278:29261–29266.
44. Chin D, Means AR. Calmodulin: a prototypical calcium sensor. Trends Cell Biol 2000;10:322–328.
45. Project E, Friedman R, Nachliel E, Gutman M. A molecular dynamics study of the effect of Ca^{2+} removal on calmodulin structure. Biophys J 2006;90:3842–3850.
46. Zhao J, Roy SA, Nelson DJ. MD simulations of anthrax edema factor: calmodulin complexes with mutations in the edema factor "switch a" region and docking of 3′-deoxy ATP into the adenylyl cyclase active site of wild-type and mutant edema factor variants. J Biomol Struct Dyn 2003;21:159–170.
47. Case DA, Darden TA, Cheatham TE, Simmerling CL, Wang J, Duke RE, Merz KM, Wang B, Pearlman DA, Crowley M, Brozell S, Tsui V, Gohlke H, Mongan J, Hornak V, Cui G, Beroza P, Schafmeister C, Caldwell JW, Ross WS, Kollman PA. AMBER 8. San Francisco: University of California; 2004.
48. Jorgensen WL. Quantum and statistical mechanical studies of liquids. 10. Transferable intermolecular potential functions for water, alcohols, and ethers. Application to liquid water. J Am Chem Soc 1981;103:335–340.
49. Symersky J, Lin G, Li S, Qiu S, Carson M, Schormann N, Luo M. Structural genomics of *Caenorhabditis elegans*: crystal structure of calmodulin. Proteins 2003;53:947–949.
50. Aqvist J. Ion-water interaction potentials derived from free energy perturbation simulations. J Phys Chem 1990;94:8021–8024.
51. Darden T, York D, Pedersen L. Particle mesh Ewald: an N.log(N) method for Ewald sums in large systems. J Chem Phys 1993;98:10089–10092.
52. Berendsen HJC, Postma JPM, van Gunsteren WF, DiNola A, Haak JR. Molecular dynamics with coupling to an external bath. J Chem Phys 1984;81:3684–3690.
53. Ryckaert JP, Ciccotti G, Berendsen HJC. Numerical integration of the cartesian equations of motion of a system with constraints: molecular dynamics of n-alkanes. J Comput Phys 1977;23:327–341.
54. Lyman E, Zuckerman DM. Ensemble-based convergence analysis of biomolecular trajectories. Biophys J 2006;91:164–172.
55. Baysal C, Atilgan AR. Relaxation kinetics and the glassiness of native proteins: coupling of timescales. Biophys J 2005;3:1570–1576.
56. Grace User's Guide, Version 5.1. Israel: Weizmann Institute of Science; 2007.
57. Pascual-Ahuir JL, Mehler EL, Weinstein H. Calmodulin structure and function: Implication of arginine in the compaction related to ligand binding. Mol Eng 1991;1:231–247.
58. Kabsch W, Sander C. Dictionary of protein secondary structure: pattern recognition of hydrogen-bonded and geometrical features. Biopolymers 1983;12:2577–2637.
59. Sanner MF, Olson AJ, Spehner JC. Fast and robust computation of molecular surfaces. In: Proc 11th ACM Symp Comp Geom C6–C7; June 5–7, 1995, Vancouver, British Columbia, Canada.
60. McDonald IK, Thornton JM. Satisfying hydrogen bonding potential in proteins. JMB 1994;238:777–793.
61. Wallace AC, Laskowski RA, Thornton JM. LIGPLOT: a program to generate schematic diagrams of protein-ligand interactions. Prot Eng 1995;8:127–134.
62. Humphrey W, Dalke A, Schulten K. VMD: visual molecular dynamics. J Mol Graph 1996;14:33–38,27–28.
63. Ihaka R, Gentleman R. R: a language for data analysis and graphics. J Comp Graph Stat 1996;5:299–314.
64. Yang C, Kuczera K. Molecular dynamics simulations of calcium-free calmodulin in solution. J Biomol Struct Dyn 2002;19:801–819.
65. Yang C, Jas GS, Kuczera K. Structure and dynamics of calcium-activated calmodulin in solution. J Biomol Struct Dyn 2001;19:247–271.
66. Amadei A, Linssen AB, Berendsen HJ. Essential dynamics of proteins. Proteins 1993;17:412–425.
67. Frederick KK, Marlow MS, Valentine KG, Wand AJ. Conformational entropy in molecular recognition by proteins. Nature 2007;448:325–329.
68. Kuboniwa H, Tjandra N, Grzesiek S, Ren H, Klee CB, Bax A. Solution structure of calcium-free calmodulin. Nat Struct Biol 1995;2:768–776.
69. Einspahr H, Bugg CE. Calcium and its role in biology. New York: M. Dekker; 1984.
70. Cates MS, Teodoro ML, Phillips GN Jr. Molecular mechanisms of calcium and magnesium binding to parvalbumin. Biophys J 2002;82:1133–1146.
71. Grabarek Z. Structure of a trapped intermediate of calmodulin: calcium regulation of efhand proteins from a new perspective. J Mol Biol. 2005;346:31351–31366.
72. Kobayashi C, Takada S. Protein grabs a ligand by extending anchor residues: molecular simulation for Ca^{2+} binding to calmodulin loop. Biophys J 2006;90:3043–3051.